Title

The effects of biodegradable and plastic film mulching on nitrogen uptake, distribution, and leaching in a drip-irrigated sandy field

Authors
Chen, Ning
Li, Xianyue
Šimůnek, Jirí
et al.

Publication Date
2020-04-01

DOI
10.1016/j.agee.2020.106817

Peer reviewed

Agriculture, Ecosystems and Environment 292 (2020) 106817

Contents lists available at ScienceDirect

Agriculture, Ecosystems and Environment

journal homepage: www.elsevier.com/locate/agee

The effects of biodegradable and plastic film mulching on nitrogen uptake, distribution, and leaching in a drip-irrigated sandy field

Ning Chen[a], Xianyue Li[a,*], Jirí Šimůnek[b], Haibin Shi[a], Zongjiang Ding[a], Yuehong Zhang[a]

[a] College of Water Conservancy and Civil Engineering, Inner Mongolia Agricultural University, Huhhot, 010018, China

[b] Department of Environmental Sciences, University of California Riverside, Riverside, CA, 92521, USA

ARTICLE INFO

Keywords:
Drip irrigation
Biodegradable film mulching
Plastic film mulching
Nitrate nitrogen
N-fertilizer application
Sandy field

ABSTRACT

Drip irrigation under plastic film mulching with applications of the N-fertilizer is an excellent agricultural strategy, resulting in saving irrigation water, improving N use efficiency, and increasing crop yield. However, the film residue and nitrate-nitrogen (NO_3-N) losses are the leading cause of non-point pollution in agricultural fields. To promote the development of sustainable agriculture, the HYDRUS (2D/3D) model was first calibrated and then validated using experimental data from 2016 and 2017, respectively, collected in the drip-irrigated sandy field with plastic film mulching (PFM), biodegradable film mulching (BFM), and no film mulching (NFM). Additionally, the NO_3-N spatial and temporal distributions, uptake, leaching, and use efficiency (NUE) under PFM, BFM, and NFM with 280 kg ha^{-1} of the N-fertilizer (the local recommendation) were evaluated using both observed and simulated data. These factors were also assessed under BFM with 210 (75 % of the recommended value) and 140 kg ha^{-1} (50 % of the recommended value) of the N-fertilizer. The results of numerical simulations were in good agreement with observations, with the *RMSE*, R^2, and *NSE* during verification being 0.01-0.08 mg cm^{-3}, 0.62-0.87, and 0.68-0.94, respectively. When the same amount of the N-fertilizer (280 kg ha^{-1}) was applied in each treatment, there were no apparent differences in NO_3-N concentrations in the soil profile, cumulative NO_3-N uptake by corn (CNU), and cumulative NO_3-N leaching (CNL) in the 100-cm soil depth between the BFM_{280} and PFM_{280} scenarios (the subscript indicates the amount of the N-fertilizer) during the early growing season (Day After Sowing [DAS] of 0–78 in 2016 and DAS of 0–92 in 2017). However, CNU and CNL were higher, and the NO_3-N concentrations in the upper soil layer (0 – 40 cm soil layer) lower in these two scenarios than in the NFM_{280} scenario. The NO_3-N concentrations in the topsoil layer (the 0 – 20 cm soil layer) in the BFM_{280} scenario were 3.9 % higher than in the PFM_{280} scenario during DAS 93–154 in 2017 due to the disintegration of the biodegradable film and 26.3 % lower during DAS 79–155 in 2016 because of intensive rainfall. Additionally, the highest NUE (50.9 kg kg^{-1}, the average value for two years) was found when 75 % of the recommended N-fertilizer (210 kg ha^{-1}) was applied. Therefore, an application of 210 kg ha^{-1} of the N-fertilizer in the BFM scenario can be recommended for sandy farmland to avoid plastic pollution, increase NUE, and effectively promote the development of sustainable agriculture.

1. Introduction

With worldwide economic development, population growth, and regional water shortages, agricultural production has, in recent years, increasingly focused on saving agricultural water and improving crop yields. Drip irrigation under plastic film mulching (PFM) has been proven to be an excellent irrigation strategy with many benefits and advantages compared to no film mulching, such as saving irrigation water (Vázquez et al., 2006), preserving soil water (Berger et al., 2013), improving soil temperature (Filipovic et al., 2016), promoting early germination and harvest (Novello and Palma, 2008), and significantly increasing crop yields (Monday et al., 2015; Ospanbayev et al., 2017; He et al., 2018). Additionally, it can be used under different climate conditions and in different soil regions (Monteiro et al., 2013; Sharma et al., 2017; Fawibe et al., 2019; Qin et al., 2019; Wang et al., 2019a,b), especially in arid, semi-arid, and sandy regions with low precipitation, high evaporation, and a limited soil water and fertilizer retention (Zhou et al., 2017; Dlamini et al., 2017). Therefore, drip irrigation under PFM has been used worldwide, including Japan (Fawibe et al., 2019), Pakistan (Nasrullah et al., 2011), Spain (Jordi et al., 1995), and China (Guo et al., 2019).

The largest user of the plastic film in the world is China (Daryanto

* Corresponding author.
E-mail address: lixianyue80@126.com (X. Li).

https://doi.org/10.1016/j.agee.2020.106817
Received 1 September 2019; Received in revised form 27 December 2019; Accepted 6 January 2020

et al., 2017), where the amount of the plastic film applied on crops has increased to 14.7 × 10^5 t, and the plastic mulching area has reached 184 × 10^5 ha (Gao et al., 2019). However, recycling of plastic film residues is a high-cost and challenging process, which causes the accumulation of plastic film residues in the soil at a rate of about 71.9-259.1 kg ha^{-1} (Liu et al., 2014; Yan et al., 2014).

Generally, most plastic films are made of low-density polyethylene that needs at least several hundred years to completely degrade in soil (Khalil et al., 2018; Henry et al., 2019). When the plastic residue in soil increases above a certain threshold value, it incurs significant negative impacts on soil environment and agricultural production, such as damaging soil structure (Gao et al., 2019), decreasing soil water infiltration (Jiang et al., 2017), retarding soil water and nutrient movement (Dong et al., 2013; Jiang et al., 2017), restricting root growth (Ibarra-Jiménez et al., 2011; Qi et al., 2018), and reducing crop yield (Dong et al., 2013; He et al., 2018; Gao et al., 2019).

Biodegradable films could effectively overcome these problems because they are mainly made of degradable materials (Henry et al., 2003), such as starch-based materials, cellulose acetate (CA), cellulose nitrate (CN), and mixed cellulose filter membrane (CN-CA) (Moreno et al., 2017; Khalil et al., 2018) that can disintegrate directly into CO_2 and H_2O by soil microbes without causing any significant environmental damage. Therefore, biodegradable films are regarded as valuable alternatives to plastic films that have been adopted in many countries, such as Norway (Touchaleaume et al., 2016), Japan (Wen, 2005), China (Wang et al., 2019a,b), and Spain (Mari et al., 2019). A large number of studies have shown that soil temperatures and soil water contents under biodegradable film mulching (BFM) were similar as under PFM during the early growing season, decreased a little during the middle crop growth stage due to the partial degradation of the biodegradable film, and decreased significantly during the late crop growth stage due to the considerable film degradation (Gu et al., 2017; Saglam et al., 2017 ; Sun et al., 2018; Wang et al., 2019a,b). Additionally, the rate of film degradation can be adjusted by altering ingredients of the biodegradable film to regulate and control soil water contents and soil temperatures during the crop growth season (Yin et al., 2019).

The effects of BFM on soil water flow and soil heat movement have been documented in many studies (Saglam et al., 2017; Sun et al., 2018; Zheng et al., 2019). However, there has been little focus on the movement of soil nitrogen under BFM, especially of NO_3-N, the most essential nutrient for crop growth. At present, the research focus is most frequently on decreasing NO_3-N leaching and increasing the N use efficiency (NUE) under PFM and no film mulching (NFM) (Ruidisch et al., 2013; Egrinya et al., 2013; Li et al., 2017), i.e., on optimizing fertigation rates, amounts, and frequency so that NO_3-N leaching to groundwater is minimized while the crop yield is increased (Filipovic et al., 2016; Zhang et al., 2012).

Mulching can significantly decrease soil evaporation and topsoil NO_3-N concentrations (Ma et al., 2018; Wang and Xing, 2016), increase nitrogen uptake by crop roots and its transport to stem, leaves, and fruits (Zheng et al., 2018), and decrease nitrogen leaching below the root zone (Ma et al., 2018). Although nitrogen movement, uptake, and leaching have been often studied both experimentally and numerically for different conditions involving different irrigation amounts, different fertilizer rates and levels, and different mulching types, these studies mainly focused on NO_3-N dynamics in either un-mulched fields or in fields mulched with the plastic (i.e., not disintegrating) film. There was very little similar research about NO_3-N dynamics under BFM. NO_3-N dynamics under BFM is significantly affected by various environmental factors due to the disintegration of the biodegradable film, especially in dripped-irrigated sandy soils. Additionally, no comparative analysis has been carried out in drip-irrigated sandy fields that would quantitatively evaluate differences in NO_3-N distributions, uptake, and leaching under different mulching types and for different N-fertilizer amounts under BFM.

Although the effects of different fertigation and mulching strategies on nitrogen could be evaluated using field experiments, this is a time-consuming and costly approach. In contrast, validated numerical models can be easily applied to find optimal mulching, irrigation, and fertigation strategies for a given soil, climate, and environmental conditions. For example, Azad et al. (2018) used the HYDRUS model simulations to show that NO_3-N leaching was minimized during the fertigation period when the irrigation rate of 0.8 Lh^{-1} and the minimum duration of fertigation at the end of irrigation were used. Similarly, Karandish and Šimůnek (2017) used HYDRUS to simulate drip irrigation for 11 irrigation levels and 8 nitrogen fertilization rates and showed that NO_3-N leaching from the topsoil layer (0 − 20 cm) increased with an increase in fertigation rates, while N uptake increased as well. They also showed that the fertilization rate of 200 kg ha^{-1} reduced NO_3-N leaching by 30 % compared to the fertigation rate of 250 kg ha^{-1}.

The specific objectives of this study therefore are: 1) to calibrate and validate HYDRUS (2D/3D) using the NO_3-N experimental data collected during the crop growing season under BFM, PFM, and NFM, 2) to compare differences and similarities in NO_3-N concentrations, their two-dimensional spatial distributions, and N balances under BFM, PFM, and NFM for the same N-fertilizer application (i.e., 280 kg ha^{-1}), and 3) to analyze N uptake, NO_3-N leaching, NUE, and N balances under BFM for three different (i.e., 280, 210, and 140 kg ha^{-1}) N-fertilizer applications.

2. Materials and methods

2.1. Field experiment

A two-year (during 2016–2017) field investigation was carried out in a 2400 m^2 (40 × 60 m) cornfield at the Muleitan experimental station (106°9′-107°10′E, 40°9′-40°57′N) located in the Ulanbuh sandy region, 50 km away from the Yellow River, China (Fig. 1a). Mean annual sunlight in the area can reach 3180 h, mean annual precipitation is 103 mm, and mean annual potential evaporation is 2259 mm. The soil in the experimental field is classified as sandy soil with an average bulk density of 1.55 g cm^{-3} (Table 1) and the average field capacity (θ_{fc}) in the 0 − 100 cm soil layer of 0.224 (the volumetric water content). Soil total nitrogen and organic matter in the upper soil layer (0 − 40 cm) were 0.3 and 5.2 g kg^{-1}, respectively, and the C:N ratio was 10.1. Available nitrogen, available potassium, and available phosphorus were 18.2, 76.9, and 5.1 mg kg^{-1}, respectively.

Corn seed (*Zea mays L*) was sown on April 28 and May 1 and harvested on September 30 and October 1 in 2016 and 2017, respectively. The planting pattern was "one film, one tube, and two rows" with crop rows 50 cm apart and the crop spacing of 30 cm (Fig. 1b). The experimental design was a completely random design comprising of three replicates of five treatments, i.e., 15 field plots. Different treatments included three mulching treatments with a locally recommended N-fertilizer application (280 kg of N per ha): plastic film mulching (PFM_{280}), biodegradable film mulching (BFM_{280}), and no film mulching (NFM_{280}), which are either impermeable, partially permeable, or fully permeable to evaporation and rainfall, respectively. The last two treatments involved BFM with an application of either 75 % or 50 % of the recommended N-fertilizer amount. There were thus three levels of applied N-fertilizer under BFM: 280 kg ha^{-1} (BFM_{280}), 210 kg ha^{-1} (BFM_{210}), and 140 kg ha^{-1} (BFM_{140}). Before sowing, 120 kg ha^{-1} of Diammonium phosphate ($(NH_4)_2HPO_4$, N ≥ 18 %), and 120 kg ha^{-1} of Potassium sulfate (K_2SO_4) were applied in the field as basal fertilizer. The Carbamide solution ($CO(NH_2)_2$, N ≥ 32 %) as topdressing was applied in the field in the elongation stage (30 % of the total N-fertilizer), the tasseling stage (30 % of the total N-fertilizer), and the filling stage (20 % of the total N-fertilizer), each time accompanied with drip irrigation. Irrigation was performed with a single line of a drip tape with an emitter discharge of 2.4 L h^{-1} and a distance between emitters

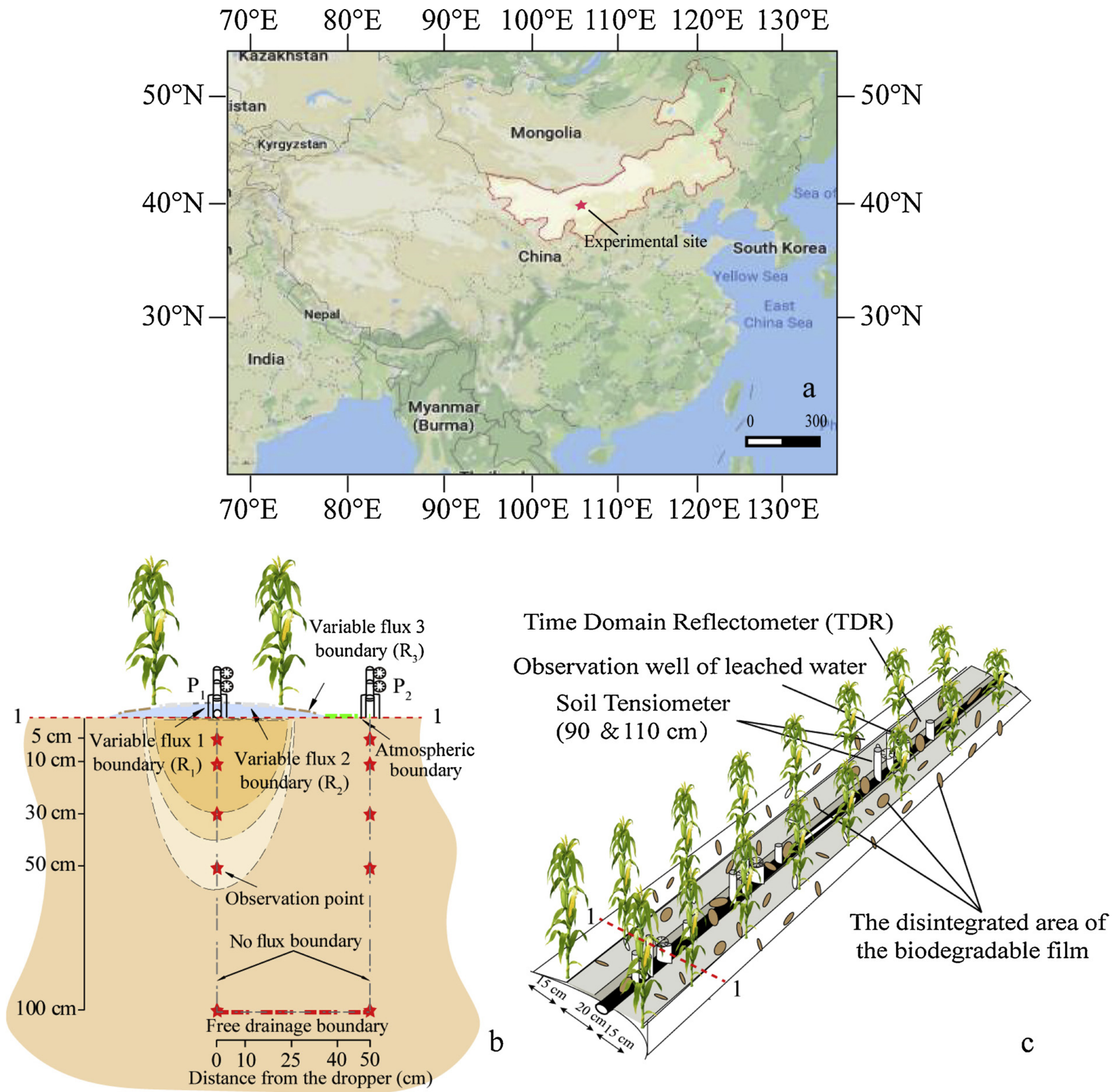

Fig. 1. The geographical location of the experimental field (a), the modeling domain, boundary conditions, and locations of sensors (P_1 and P_2) (b), and the cropping pattern (c) under biodegradable film mulching (BFM).

of 30 cm. The water meter (with an accuracy of 0.001 L) was set up to monitor water flow. The same irrigation amount (30 mm for each irrigation event) was applied to each plot once every 7–15 days, and 11 and 13 irrigation events were used throughout the growing seasons of 2016 and 2017, respectively.

2.2. Field monitoring

Meteorological data in the experimental field, including daily precipitation, solar radiation, air temperatures, air humidity, and wind speed, were collected using the automatic meteorological station (Onset Computer Inc.; U30, Hobo, USA). Reference crop evapotranspiration (ET_0) was then calculated using the Penman-Monteith approach (Monteith, 1981). Daily potential evapotranspiration rates were

Table 1
Soil physical properties and soil hydraulic parameters (the residual water content θ_r, the saturated water content θ_s, the shape parameters (α, n, and l), and the saturated hydraulic conductivity K_s) of the three soil layers of the experiment field.

Depth (cm)	Soil particle size distributions (%)			Soil texture	Bulk density	θ_r	θ_s	α	n	K_s	l
	Clay	Silt	Sand		(g m^{-3})	(cm^3 cm^{-3})	(cm^3 cm^{-3})	(cm^{-1})	(-)	(cm day^{-1})	(-)
0-20	8.6	2.9	88.5	Sand	1.58	0.049	0.371	0.035	1.63	63.4	0.5
20–40	8.5	2.2	89.3	Sand	1.59	0.049	0.367	0.035	1.81	94.7	0.5
40–100	7.2	2.7	90.1	Sand	1.41	0.061	0.426	0.029	2.03	214.9	0.5

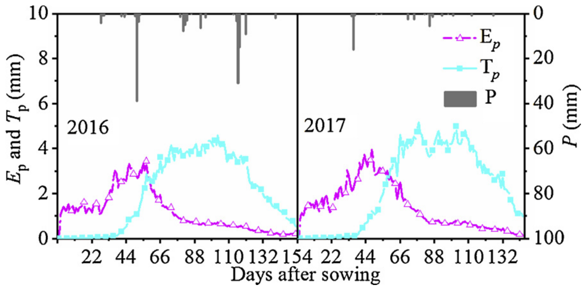

Fig. 2. Potential evaporation (E_p), potential transpiration (T_p), and precipitation (P) during the 2016 and 2017 growing seasons.

calculated by multiplying ET_0 by K_c (the crop coefficient) that were taken from the FAO paper (No.56) for corn, i.e., 0.30 during the early season, 1.2 during the mid-season, and 0.35 during the later season (Allen et al., 1998). Additionally, potential evaporation (E_p) and transpiration (T_p) fluxes were calculated from potential evapotranspiration using Beer's law (Campbell and Norman, 1989) (Fig. 2).

Soil water contents (SWCs) were measured using TDR probes (IMKO GmbH Inc., IPH, TRIME-PICO, Germany), which were installed under the drip tape (P_1) and in the middle of two rows of corn (P_2) (Fig. 1b). TDR measurements were taken once every 5–7 days at soil depths of 0–10, 10–20, 20–40, 40–60, and 60 – 100 cm. Additionally, a soil auger (Beijing New Landmark Soil Equipment Co., Ltd., 0301, XDB, CHN) was used to obtain soil samples to measure SWCs at periodic intervals. SWCs measured using TDR probes were further verified using the measurements on soil samples (Skaggs et al., 2004).

Soil sampling locations for NO_3-N concentrations were the same as for SWCs, and the sampling interval was about every two weeks. Soil NO_3-N concentrations were measured using the semi-micro Kjeldahl method (Bremner and Keeney, 1965). Soil samples were shaken with 2 mol L^{-1} KCl (1:5 soil: solution ratio) for 1 h, and the obtained extract was analyzed using an ultraviolet spectrophotometer (Beijing General Instrument Co. LTD., TU-1901, General Instrument, CHN). Total N uptake (in the corn stem, leaves, and grain) was determined on the same dates; these samples were first kept for 30 min at 105℃ temperature and then conserved at 75℃ temperature in the oven to reach a constant weight. After crushing and sieving, a 0.2 g sample was weighted by a weighing paper, digested with 5 mL of concentrated H_2SO_4, and measured by a flow analyzer (Brown ruby Inc., AA3, SEAL, Germany). The semi-micro Kjeldahl method (Bremner and Keeney, 1965) was applied to determine N uptake.

Self-made field lysimeters and a PVC tube opened at the bottom installed at a depth of 100 cm below the soil surface were used to measure vertical water fluxes and soil solutions before corn seeding (Li et al., 2014, 2015a,b). It was necessary to clean the residual solution in each instrument before each sampling, and the samples were collected once every 7–15 days throughout the growing season. Cumulative NO_3-N leaching (CNL) during particular time intervals was determined by multiplying the NO_3-N concentration of the leaching solution by corresponding water fluxes.

The leaf area meter (Li-3000, LI – COR, USA) and a tape (with an accuracy of 0.1 cm) were used to measure the corn leaf area and height, respectively, once every 7–15 days and the leaf area index (*LAI*) was calculated using the FAO method (Allen et al., 1998). Root samples were collected from a soil transect utilizing a method of Li et al. (2017) on June 12, June 25, July 11, and August 16 in 2016 and on June 8, June 25, July 18, and August 20 in 2017. These samples were first washed off and then scanned using the WinRHIZO software. When crops reached physiological maturity, ten plants from each plot were randomly harvested to determine the grain number per cob and the 100-grain weight in the harvesting area of 20 m^2 (Mueller and Vyn, 2018).

Since the disintegrated area of the biodegradable film varied in the direction perpendicular to the drip tape, the mulching region was divided into three parts R_1, R_2, and R_3 (Fig. 1b), and was photographed using a digital camera (Canon EOS Rebel T3, Japan) from a distance of about 25 cm between the camera and the surface of the biodegradable film under daylight conditions once every 20 days (Chen et al., 2019). Images were processed using a geometric correction and a background subtraction, and the average disintegrated area of the biodegradable film in both years was calculated using the Auto CAD 2010 software (Autodesk Inc., USA). The disintegrated area was 13.1, 5.2, and 1.2 % on day 60 after sowing in regions R_1, R_2, and R_3, respectively, 26.5, 11.5, and 6.8 % after 80 days, 48.3, 28.5, and 10.2 % after 100 days, 83.0, 37.6, and 16.5 % after 120 days, 100, 46.6, and 20.7 % after 140 days, and 100, 53.0 and 26.1 % on the last day of the experiment (DAS 155 for 2016 and DAS 154 for 2017). Values for other days were obtained using linear interpolation. The disintegration of the plastic film was negligible compared with that of the biodegradable film, and it was ignored in the simulation.

2.3. Modeling software and input parameters

2.3.1. Governing equations of water flow and solute transport

Numerical modeling of soil water flow and solute transport was performed using the HYDRUS (2D/3D) software (Šimunek et al., 2016) for appropriate initial and boundary conditions and soil heterogeneities in the two-dimensional domain (Fig. 1b). Water flow dynamics in a variably-saturated porous medium was solved using a numerical solution of the Richards equation, which was defined as:

$$\frac{\partial \theta}{\partial t} = \frac{\partial}{\partial x}\left[K(h)\frac{\partial h}{\partial x}\right] + \frac{\partial}{\partial z}\left[K(h)\left(\frac{\partial h}{\partial z} + 1\right)\right] - S(h) \tag{1}$$

where θ is the volumetric water content ($cm^3\ cm^{-3}$), h is the pressure head (cm), K is the unsaturated hydraulic conductivity (cm day^{-1}), t is time (day), S is the root water uptake term ($cm^3\ cm^{-3}\ day^{-1}$), x is the horizontal coordinate, and z is the vertical coordinate. Actual root water uptake S is calculated using the potential uptake rate and a water stress factor (Feddes et al., 1978):

$$S(h) = \alpha(h) \cdot b(x, z, t) \cdot T_p L_T \tag{2}$$

where $\alpha(h)$ is a dimensionless stress response function (-), T_p is the potential transpiration rate (cm day^{-1}), $b(x,z,t)$ is the normalized root water uptake distribution function (cm^{-2}), and L_T is the length of the soil surface associated with transpiration (cm).

The solute transport equations (for NH_4-N and NO_3-N) consider the advective-dispersive transport in the liquid phase. In this study, the partial differential equations governing non-equilibrium transport of solutes involved in a sequential first-order decay chain during transient water flow in variably-saturated rigid porous media are simplified as follows (Šimůnek et al., 2016):

For NH_4-N:

$$\begin{aligned} \frac{\partial \theta c_1}{\partial t} + \rho\frac{\partial s_1}{\partial t} = & \frac{\partial}{\partial x}\left(\theta D_{xx}\frac{\partial c_1}{\partial x}\right) + \frac{\partial}{\partial x}\left(\theta D_{xz}\frac{\partial c_1}{\partial z}\right) + \frac{\partial}{\partial z}\left(\theta D_{zx}\frac{\partial c_1}{\partial x}\right) \\ & + \frac{\partial}{\partial z}\left(\theta D_{zz}\frac{\partial c_1}{\partial z}\right) - \\ & -\left(\frac{\partial q_x c_1}{\partial x} + \frac{\partial q_z c_1}{\partial z}\right) - \mu_l \theta c_1 - \mu_s \rho s_1 - S_c 1 \end{aligned} \tag{3}$$

For NO_3-N:

$$\begin{aligned} \frac{\partial \theta c_2}{\partial t} = & \frac{\partial}{\partial x}\left(\theta D_{xx}\frac{\partial c_2}{\partial x}\right) + \frac{\partial}{\partial x}\left(\theta D_{xz}\frac{\partial c_2}{\partial z}\right) + \frac{\partial}{\partial z}\left(\theta D_{zx}\frac{\partial c_2}{\partial x}\right) + \frac{\partial}{\partial z}\left(\theta D_{zz}\frac{\partial c_2}{\partial z}\right) - \\ & -\left(\frac{\partial q_x c_2}{\partial x} + \frac{\partial q_z c_2}{\partial z}\right) + \theta \mu c_1 - S_c 2 \end{aligned} \tag{4}$$

where θ is the soil water content ($cm^3\ cm^{-3}$), ρ is the bulk density of the soil (g cm^{-3}), s_1 is the adsorbed concentration of NH_4-N (mg g^{-1}), D_{xx}, D_{xz}, D_{zx}, and D_{zz} are the components of the effective dispersion coefficient tensor (cm^2 D^{-1}), c is the solute concentration (NH_4-N or NO_3-N) in the liquid phase (mg cm^{-3}), q_x and q_z are the components of the volumetric flux density (cm d^{-1}), μ_l and μ_s are the first-order reaction rate constants representing the nitrification process (d^{-1}) in the liquid and solid phases, respectively, and S is a sink term (d^{-1}). Eqs. (3) and (4) in general include the solute flux due to dispersion, the solute flux due to convection with flowing water, and nutrient uptake by roots, S_c (mg cm^{-3} d^{-1}), which is associated with root water uptake S:

$$S_c1 = S(h)c_1 \qquad S_c2 = S(h)c_2 \tag{5}$$

where c_1 and c_2 are the NH_4-N and NO_3-N concentrations taken up by roots (mg cm^{-3}).

2.3.2. Initial and boundary conditions

The two-dimensional transport domain was defined as a rectangle with a width of 50 cm and a depth of 100 cm (Fig. 1b). The SWC initial condition was based on measured values. Due to the soil texture of sandy soils that retained little water, the initial values of NH_4-N and NO_3-N could be neglected. The initial values of NH_4-N and NO_3-N thus only reflected the initial application of the basal fertilization. The horizontal distribution of initial water contents and solute concentrations was assumed to be uniform.

The boundary conditions at the upper boundary included up to three time-variable fluxes and one atmospheric boundary condition to represent drip irrigation and to apply precipitation, evaporation, and transpiration fluxes. Three different sets of boundary conditions were specified for three mulching scenarios with a biodegradable film, a plastic film, and no film (Chen et al., 2019). In the scenarios with a biodegradable film (i.e., BFM_{280}, BFM_{210}, and BFM_{140}), the mulched soil surface (0 − 40 cm) was divided into three parts (Fig. 1b) to represent uneven disintegration of the biodegradable film: the soil surface up to 10 cm away from the emitter (R_1) with the highest disintegration was assigned a "Variable Flux 1″ boundary condition; the 10 − 25 cm soil surface (R_2) was assigned a "Variable Flux 2″ boundary condition, the 25 − 40 cm soil surface (R_3) with the lowest disintegration was assigned a "Variable Flux 3″ boundary condition, and the 40 − 50 cm soil surface with no film was assigned an "Atmospheric" boundary condition. In the scenario with a plastic film (i.e., PFM_{280}), the mulched soil surface (0 − 40 cm) was assigned a "No Flow" boundary condition and the 40 − 50 cm soil surface without mulch was assigned an "Atmospheric" boundary condition. In the scenario without mulching (i.e., NFM_{280}), the entire soil surface (0 − 50 cm) was assigned an "Atmospheric" boundary condition. The emitter flux specified along a 0.8 cm long boundary was calculated using the following equation (Skaggs et al., 2004):

$$q = \frac{Q}{L \times 2\pi r} \tag{6}$$

where q is the emitter flux (15.9 cm h^{-1}), Q is the emitter discharge (2.4 L h^{-1}), L is the distance between emitters (30 cm), and r is the radius of the emitter (0.8 cm).

A "Free Drainage" boundary condition, allowing for downward drainage, was applied along the bottom boundary of the transport domain since the groundwater table was over 300 cm deep during the growing season and did not affect flow in the transport domain. Due to flow symmetry, a "No Flow" boundary condition was specified along vertical (left and right) boundaries. The third-type Cauchy boundary condition was used for solute transport along all boundaries with specified water fluxes (at the top boundary), while the second-type Neumann boundary condition was used for solute transport along outflow boundaries (at the bottom boundary).

2.3.3. Modeling parameters

Soil hydraulic parameters for the van Genuchten-Mualem model for different soil layers (0–20, 20–40, and 40 − 100 cm) were estimated using the Rosetta software package (Schaap et al., 2001). The initial estimates of soil hydraulic parameters were based on the soil textural distribution (i.e., percentages of sand, silt, and clay) and the bulk density. These initial estimates of soil hydraulic parameters (α, n, and K_s) for the three different soil layers were further calibrated using an inverse modeling technique (Lazarovitch et al., 2009). The calibrated values of soil hydraulic parameters are shown in Table 1.

The solute transport in HYDRUS (2D/3D) is a relatively complex process that may include nitrification, denitrification, volatilization, immobilization, and mineralization. In this study, the denitrification process was neglected because such a reaction mainly occurs under saturated conditions (Ravikumar et al., 2011). Additionally, immobilization and mineralization in the sandy soil were also neglected, similarly as in many other studies (e.g., Ramos et al., 2012; Tafteh and Sepaskhah, 2012). Meanwhile, ammonia volatilization was also neglected since fertilizers were applied with irrigation water; a similar assumption was made in previous studies (e.g., Ramos et al., 2012). On the other hand, the applied fertilizer ammonium nitrogen (NH_4-N) transforms first into NO_2-N, and then further to NO_3-N. Since the residual concentration of NO_2-N in the soil profile was low, and nitrification of NO_2-N to NO_3-N is a relatively fast process, it can be assumed that NH_4-N transforms directly into NO_3-N, which is consistent with many other studies (e.g., Wang et al., 2010; Tafteh and Sepaskhah, 2012). This study also assumed that NO_3-N did not adsorb and existed only in the dissolved phase, while ammonium NH_4-N adsorbed and was present in both solid and dissolved phases. The distribution coefficient (K_d) were set to 0 and 3.5 cm^3 g^{-1} for NO_3-N and NH_4-N, respectively (Hanson et al., 2006). The first-order rate (nitrification) constants for solutes in the liquid and solid phases in the sandy soil were set to 0.03 and 0.16 d^{-1}, respectively (Castaldelli et al., 2018).

In the solute transport equation of HYDRUS (2D/3D), components of the dispersion tensors are calculated using longitudinal and transversal dispersivities (D_L and D_T, respectively) of the soil and the molecular diffusion coefficient of the solute in free water. Longitudinal dispersivities (D_L) were considered to be 20 cm in the 0 − 20 cm soil layer, 10 cm in the 20 − 40 cm soil layer, and 5 cm in the 40 − 100 cm soil layer. Transverse dispersivities (D_T) were assumed to be one-tenth of D_L (e.g., Cote et al., 2003; Hanson et al., 2006; Ramos et al., 2012). The molecular diffusion coefficients of NH_4-N and NO_3-N in free water were set to be 0.064 and 0.068 cm^2 h^{-1}, respectively (Cote et al., 2003; Nakamura et al., 2004). Finally, c_{smax}, the maximum allowed concentration for root nutrient uptake (Šimunek et al., 2016), was obtained by comparing simulated and observed values of crop N uptake.

2.4. Statistical analysis

Significant differences in yield for different treatments were analyzed using the SPSS software (SPSS Inc., 20.0., USA). The root mean square error (*RMSE*), the determination coefficient (R^2), and the Nash-Sutcliffe efficiency (*NSE*) were used to evaluate the model performance in simulating soil water contents (SWC) and solute concentrations (NO_3-N):

$$RMSE = \sqrt{\frac{1}{n}\sum_{i=1}^{n}(S_i - O_i)^2} \tag{7}$$

$$R^2 = \frac{\sum_{i=1}^{n}(O_i - \bar{O})(S_i - \bar{S})}{\sqrt{\sum_{i=1}^{n}(O_i - \bar{O})}\sqrt{\sum_{i=1}^{n}(S_i - \bar{S})}} \tag{8}$$

$$NSE = 1 - \frac{\sum_{i-1}^{n}(S_i - O_i)^2}{\sum_{i-1}^{n}(O_i - \bar{O})^2} \tag{9}$$

where S_i is the simulated soil water content (cm^3 cm^{-3}) or NO_3-N concentration (mg cm^{-3}), O_i is the corresponding observed soil water content (cm^3 cm^{-3}) or NO_3-N concentration (mg cm^{-3}), n is the

Table 2
Statistical results for HYDRUS (2D/3D) calibration (2016) and validation (2017) for soil water contents (SWC) and NO_3-N concentrations (NC) of different soil layers under different mulching scenarios (PFM, BFM, and NFM) and N-fertilizer applications (subscripts 140, 210, and 280 kg ha^{-1}). *RMSE*, R^2, and *NSE* are the root mean square error, the coefficient of determination, and the Nash-Sutcliffe efficiency, respectively.

Year	Parameter	Depth (cm)	PFM_{280}			BFM_{280}			BFM_{210}			BFM_{140}			NFM_{280}		
			RMSE	R^2	*NSE*	*RMSE*	R^2	*NSE*	*RMSE*	R^2	*NSE*	*RMSE*	R^2	*NSE*	*RMSE*	R^2	*NSE*
2016	SWC (cm^3 cm^{-3})	0–10	0.03	0.83	0.85	0.03	0.80	0.84	0.03	0.82	0.85	0.03	0.85	0.90	0.05	0.72	0.81
		10–20	0.02	0.85	0.92	0.03	0.82	0.87	0.03	0.87	0.88	0.02	0.84	0.87	0.04	0.78	0.85
		20–40	0.03	0.81	0.94	0.04	0.78	0.82	0.02	0.84	0.91	0.04	0.81	0.85	0.04	0.76	0.82
		40–60	0.01	0.88	0.95	0.02	0.85	0.92	0.02	0.88	0.94	0.02	0.87	0.95	0.03	0.82	0.89
		60–100	0.01	0.91	0.98	0.01	0.88	0.94	0.01	0.89	0.97	0.01	0.88	0.99	0.02	0.85	0.88
	NC (mg cm^{-3})	0–10	0.05	0.78	0.82	0.06	0.76	0.80	0.05	0.74	0.80	0.03	0.82	0.84	0.07	0.65	0.72
		10–20	0.04	0.80	0.85	0.06	0.81	0.83	0.03	0.82	0.85	0.03	0.83	0.87	0.06	0.68	0.76
		20–40	0.04	0.79	0.87	0.05	0.73	0.82	0.03	0.80	0.88	0.04	0.78	0.84	0.05	0.72	0.84
		40–60	0.02	0.83	0.91	0.03	0.81	0.88	0.03	0.82	0.91	0.03	0.84	0.95	0.03	0.82	0.87
		60–100	0.01	0.85	0.92	0.01	0.82	0.91	0.02	0.83	0.98	0.01	0.88	0.97	0.02	0.83	0.90
2017	SWC (cm^3 cm^{-3})	0–10	0.04	0.76	0.81	0.04	0.73	0.78	0.04	0.71	0.80	0.03	0.72	0.81	0.06	0.71	0.78
		10–20	0.03	0.78	0.85	0.03	0.76	0.84	0.03	0.74	0.82	0.03	0.78	0.83	0.05	0.69	0.83
		20–40	0.03	0.76	0.89	0.04	0.72	0.80	0.03	0.82	0.84	0.04	0.76	0.82	0.04	0.75	0.81
		40–60	0.02	0.82	0.93	0.02	0.81	0.91	0.02	0.84	0.85	0.03	0.81	0.85	0.03	0.78	0.85
		60–100	0.01	0.85	0.94	0.01	0.84	0.93	0.01	0.85	0.87	0.02	0.85	0.87	0.03	0.81	0.86
	NC (mg cm^{-3})	0–10	0.05	0.75	0.78	0.06	0.72	0.80	0.06	0.71	0.81	0.06	0.68	0.72	0.08	0.62	0.68
		10–20	0.05	0.73	0.82	0.05	0.75	0.84	0.05	0.73	0.82	0.05	0.75	0.83	0.06	0.68	0.71
		20–40	0.04	0.77	0.86	0.05	0.74	0.81	0.05	0.78	0.85	0.05	0.71	0.81	0.06	0.65	0.70
		40–60	0.03	0.81	0.88	0.03	0.79	0.85	0.03	0.81	0.84	0.04	0.75	0.84	0.05	0.72	0.78
		60–100	0.01	0.82	0.91	0.01	0.80	0.89	0.02	0.80	0.83	0.02	0.78	0.80	0.03	0.75	0.82

number of observed values, and $\bar{S}$ and $\bar{O}$ are mean values of simulated and observed soil water contents (cm^3 cm^{-3}) or NO_3-N concentrations (mg cm^{-3}), respectively. The *RMSE* is close to zero when only small differences between simulated and observed values exist, and R^2 is close to one when a close correlation between simulated and observed values exist. Finally, *NSE*, which ranges from $-\infty$ to 1, indicates the consistency between simulated and observed values.

3. Results

3.1. Efficiency of HYDRUS (2D/3D) to simulate the NO_3-N movement

The soil hydraulic and solute dispersion parameters were first calibrated using the observed SWC and NO_3-N concentration data from different treatments and different soil depths in 2016 and then validated using corresponding 2017 data. The results showed that HYDRUS (2D/3D) could well capture temporal and spatial trends in SWCs with *RMSE* ranging from 0.01 to 0.06 cm^3 cm^{-3}, R^2 ranging from 0.69 to 0.91, and *NSE* ranging from 0.78 to 0.99 during the calibration period (Table 2, Fig. 3). The agreement between observed and simulated NO_3-N concentrations during the validation period was similarly good, with *RMSE*, R^2, and *NSE* ranging from 0.01 to 0.08 mg cm^{-3}, 0.62 to 0.87, and 0.68 to 0.94, respectively (Table 2), indicating that HYDRUS (2D/3D) can be used to simulate the movement of soil water and NO_3-N for different film mulching and N-fertilizer scenarios.

The NO_3-N concentrations increased immediately after the application of the N-fertilizer and then gradually decreased with time. The four NO_3-N concentration peaks due to one application of the base fertilizer at the beginning of the experiment and three topdressings during the growing season can be seen in Fig. 3. Mulching directly influences infiltration of rainfall and the loss of soil water from the topsoil ($0-20$ cm) due to evaporation, which primarily affects the NO_3-N distribution in the soil profile. There was almost no difference in NO_3-N concentrations in all soil layers between the PFM_{280} and BFM_{280} scenarios during DAS 0–78 in 2016 and DAS 0–92 in 2017 due to the low disintegration of the biodegradable film. However, the NO_3-N concentration under the film mulching treatments (PFM_{280} and BFM_{280}) were significantly lower than under NFM_{280}, the average NO_3-N concentrations in 2016 and 2017 for the BFM_{280}, PFM_{280}, and NFM_{280} scenarios in the $0-100$ cm soil layer were 0.078, 0.077, and 0.110 mg cm^{-3}, respectively. The disintegration of the biodegradable film (which was higher than of the plastic film) during the second half of the growing season (during DAS 79–155 in 2016 and DAS 93–154 in 2017) allowed higher soil evaporation in the BFM_{280} scenario than in the PFM_{280} scenario, which subsequently caused NO_3-N concentrations in the upper soil layer ($0-40$ cm) to be on average 5.4 % higher under BFM_{280} than under PFM_{280}, and just the opposite in the deep soil layer ($40-100$ cm).

There was intensive rainfall in this period in 2016, which decreased NO_3-N concentrations in the upper soil layer and increased them in the deeper soil layers under BFM_{280} (Fig. 3). The NO_3-N concentration after intensive rainfall was 26.3 % lower in the upper soil layer under BFM_{280} than under PFM_{280}, and 14.7 % higher in the deep soil layer. Soil evaporation in the NFM_{280} scenario was significantly higher than in the PFM_{280} and BFM_{280} scenarios, which caused NO_3-N concentrations in the upper soil layer under NFM_{280} to increase 6.3 % and 11.7 % compared with BFM_{280} and PFM_{280}, respectively, despite substantial rainfall infiltration under NFM_{280}. NO_3-N concentrations in the deep soil layer under NFM_{280} were, in general, lower than under BFM_{280} and PFM_{280}, except after a significant rainfall event on DAS 117 in 2016 (Fig. 3).

NO_3-N concentrations in different soil layers increased as a result of higher applications of the N-fertilizer under BFM_{280} compared to under BFM_{210} and BFM_{140} (Fig. 3). The average NO_3-N concentrations in the soil profile (the $0-100$ cm soil layer) under BFM_{280}, BFM_{210}, and BFM_{140} in 2016 were 0.073, 0.055, and 0.036 mg cm^{-3}, respectively, and in 2017 they were 0.073, 0.055, and 0.036 mg cm^{-3}, respectively. Overall, the soil profile NO_3-N concentrations were 11.7 %, 12.7 %, and 8.3 % lower on average in 2016 than in 2017 under BFM_{280}, BFM_{210}, and BFM_{140}, respectively, which was likely caused by intensive rainfall in 2016, which leached NO_3-N into the deeper soil layer (below 100 cm).

3.2. Effects of rainfall and N-fertilizer applications on the two-dimensional distribution of NO_3-N

Different mulching areas during the late growing season in scenarios PFM_{280}, BFM_{280}, and NFM_{280} greatly affected NO_3-N distributions in the soil profile. Since the effects of the N-fertilizer application and rainfall on soil NO_3-N distributions were similar in 2016 and 2017, only

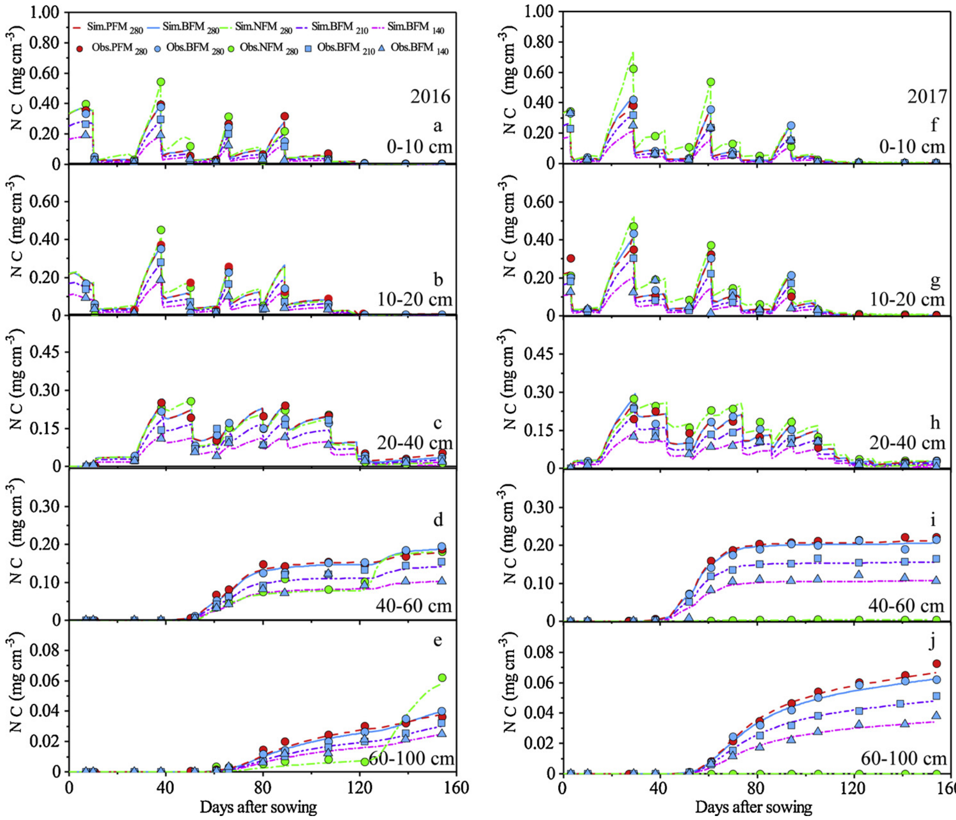

Fig. 3. Simulated and observed NO_3-N concentrations (NC) at the P_1 position in the 0–10 (a, f), 10–20 (b, g), 20–40 (c, h), 40–60 (d, i) and 60 − 100 cm (e, *j*) soil depths in 2016 (left) and 2017 (right) under plastic film mulching (PFM_{280}), biodegradable film mulching (BFM_{280}), and no film mulching (NFM_{280}) with an application of 280 kg ha^{-1} of the N-fertilizer, and biodegradable film mulching with applications of 210 kg ha^{-1} (BFM_{210}) and 140 kg ha^{-1} (BFM_{140}) of the N-fertilizer.

the results of 2016 are discussed below. Two-dimensional soil NO_3-N distributions under different mulching and N-fertilizer scenarios on DAS 79 (i.e., one day before the N-fertilizer application), DAS 82 (i.e., two days after the N-fertilizer application), DAS 116 (i.e., one day before rainfall), and DAS 118 (i.e., one day after rainfall) in 2016 are shown in Fig. 4. Most NO_3-N is concentrated in the upper soil layer (0 − 40 cm), especially in the topsoil (0 − 20 cm) and alleyways (the middle section between two rows), when less soil surface is mulched. For example, NO_3-N concentrations in the upper soil layer were 4.9 % higher under BFM_{280} than under PFM_{280} on DAS 79, and 34.0 % lower than under $NFM_{280.}$ Two days after the application of the N-fertilizer (DAS 82), NO_3-N concentrations under BFM_{280}, PFM_{280}, and NFM_{280} increased, with average NO_3-N concentrations in the upper soil layer being 0.241, 0.223, and 0.314 mg cm^{-3}, respectively.

The "available nitrate concentration" ($0 < c_{smax} < 0.4$ mg cm^{-3}, which was discussed in 2.3.3 section) under BFM_{280}, PFM_{280}, and NFM_{280} accounted for 93.6 %, 100 %, and 68.2 %, respectively, of the total soil NO_3-N in the upper soil layer. There were only slight differences in the 'available nitrate concentration' distributions two days after N-fertilizer application between BFM_{280} and PFM_{280}, but significant differences compared to NFM_{280}.

Intensive rainfall greatly affected soil NO_3-N distributions (on DAS 118). NO_3-N concentrations under BFM_{280}, PFM_{280}, and NFM_{280} in the upper soil layer one day after rain (DAS 118) decreased by 41.7 %, 29.2 %, and 74.9 %, respectively, compared to one day before rain (DAS 116) (Fig. 4 p-o), while they increased by 29.8 %, 18.5 %, and 49.3 % in the deep soil layer (40 − 100 cm), respectively, because of rainfall infiltration. Moreover, there were similar relative NO_3-N distributions for different amounts of the N-fertilizer application under BFM. NO_3-N concentrations under BFM_{210} and BFM_{140} in the upper soil layer were 24.5 % and 43.9 % lower, respectively than under BFM_{280} two days after the N-fertilizer application (DAS 82), while they decreased by 23.1 % and 40.8 %, respectively, one day after rainfall (DAS 118). A positive linear correlation ($y = 0.0003x - 0.0043$, $R^2 = 0.99$) can be found between the NO_3-N concentration in the 0 − 100 cm soil layer and the application of the N-fertilizer.

3.3. Cumulative N uptake and leaching

Both simulated and measured N uptake was very low during the early growing season (DAS 0–78 in 2016 and DAS 0–92 in 2017), then increased rapidly in the mid-season, and finally decreased again after DAS 116 in 2016 and DAS 125 in 2017 (Fig. 5a and b). In general, an increase in N uptake corresponded with an increase in the mulched area in the order of PFM_{280} (largest), BFM_{280}, and NFM_{280} (smallest). Meanwhile, there was almost no difference in cumulative N uptake (CNU) between BFM_{280} and PFM_{280} before DAS 78 in 2016 and DAS 92 in 2017, which was significantly higher than under NFM_{280} (Fig. 5a and b). The difference between BFM_{280} and PFM_{280} quickly increased after DAS 78 in 2016 and DAS 92 in 2017. Average CNU on the last day (DAS 155 and DAS 154, respectively) in 2016 and 2017 under PFM_{280} was 10.3 % and 41.4 % higher than under BFM_{280} and NFM_{280}, respectively. The average daily N uptake intensity in 2016 and 2017 under BFM_{280}, PFM_{280}, and NFM_{280} was 1.1, 1.2, and 0.9 kg ha^{-1} d^{-1}, respectively, during the early growing season, 1.9, 2.1, and 1.6 kg ha^{-1} d^{-1}, respectively, during the middle growing season (DAS 79–116 in 2016; DAS 93–125 in 2017), and 0.3, 0.4, and 0.2 kg ha^{-1} d^{-1} during the late growing season (DAS 117–155 in 2016; DAS 126–154 in 2017). The order of the N uptake intensity was similar to CNU, i.e., $PF_{280} > BF_{280} > NF_{280}$.

There were similar results for NO_3-N leaching and N uptake throughout the growing season. Average CNL in 2016 and 2017 under BFM_{280} and PFM_{280} were 8.3 and 8.6 kg ha^{-1} higher, respectively than under NFM_{280} (Fig. 5c and 5d) during the early growing season. During the middle growing season, average CNL in both years under BFM_{280}, PFM_{280}, and NFM_{280} were 16.6, 17.1, and 2.7 kg ha^{-1}, respectively, while average daily CNL was 0.4, 0.4, and 0.1 kg ha^{-1} d^{-1}, respectively. Additionally, intensive rainfall (DAS 117 in 2016) under NFM_{280} resulted in a 43.8 % higher nitrate flux to the groundwater compared with PFM_{280}. Average daily NO_3-N leaching under BFM_{280}, PFM_{280}, and

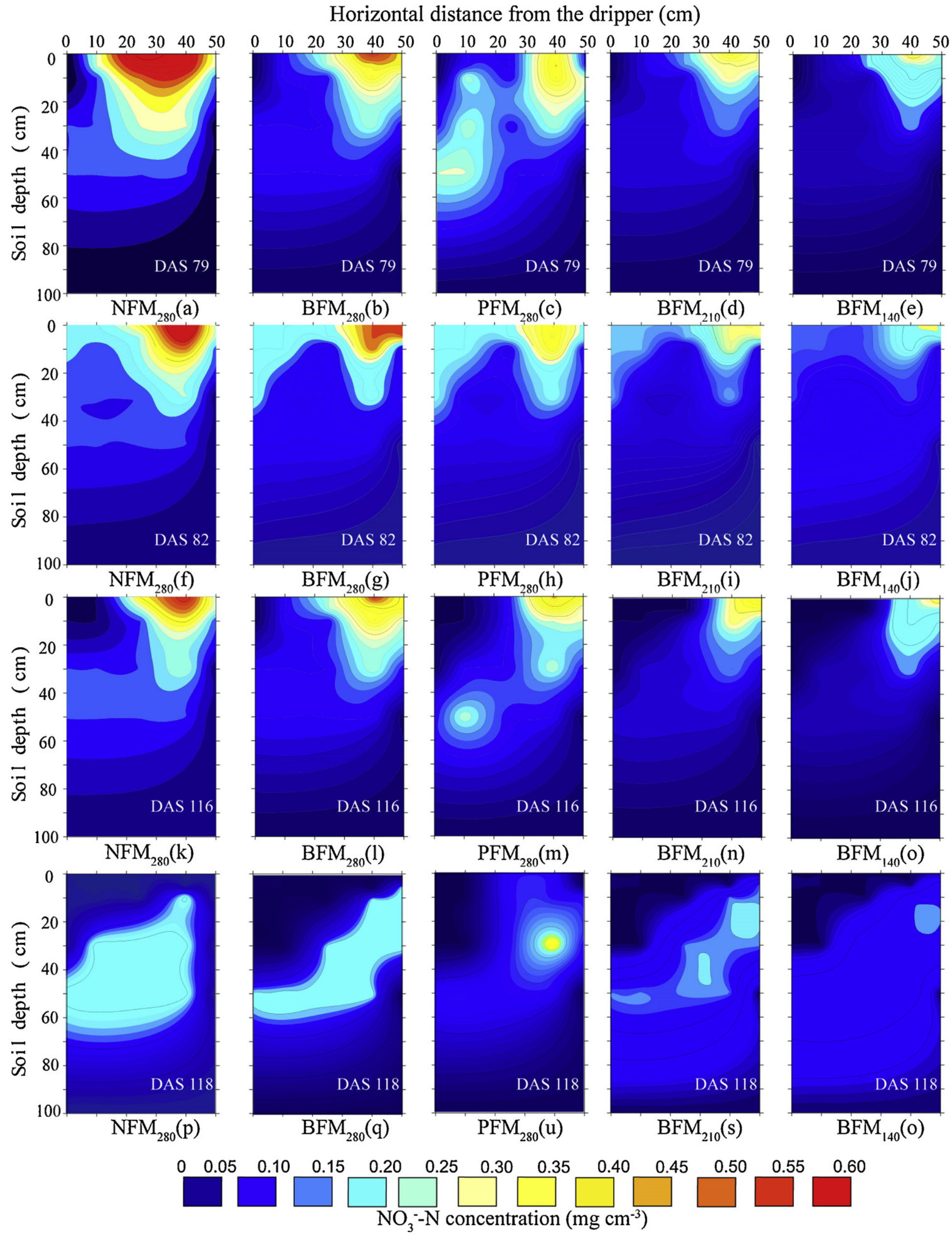

Fig. 4. Simulated two-dimensional NO_3-N distributions on DAS 79 (top; 1 day before the N-fertilizer application), DAS 82 (2 day after the N-fertilizer application), DAS 116 (1 day before rainfall), and DAS 118 (bottom; 1 day after rainfall) under plastic film mulching (middle; PFM_{280}), biodegradable film mulching (second left; BFM_{280}), and no film mulching (left; NFM_{280}) with an application of 280 kg ha^{-1} of the N-fertilizer, and under biodegradable film mulching with applications of 210 kg ha^{-1} (second right; BFM_{210}) and 140 kg ha^{-1} (right; BFM_{140}) of the N-fertilizer.

NFM_{280} were 0.7, 0.5, and 2.4 kg ha^{-1} d^{-1}, respectively, in 2016, but only 0.04, 0.1, and 0.01 kg ha^{-1} d^{-1}, respectively, in 2017 during the late growing season (Fig. 5d). Thus, PFM_{280} can increase N uptake but may cause more NO_3-N leaching out of the root zone and have detrimental effects on the soil environment. Compared with PFM_{280} and NFM_{280}, BFM_{280} not only increased N uptake, but also decreased NO_3-N leaching, and thus represented an optimal strategy.

There were apparent differences in both CNU and CNL for different applications of the N-fertilizer (Fig. 5). When the amount of N-fertilizer decreased by 25 %, and CNU and CNL decreased by 25.8 % and 23.1 %, respectively. Correspondingly, a 50 % decrease in the applied N-fertilizer produced reductions of 51.8 % and 36.2 % in CNU and CNL, respectively.

3.4. Components of the N balance and the N use efficiency

The N use efficiency (NUE) is a critical index in the agricultural production that is affected by many factors such as nitrification, CNU, CNL, and crop yield. When the same amounts of the N-fertilizer and irrigation were applied, a decrease in the mulching area resulted in enhancing nitrification, which may be caused by receiving more rainwater. The nitrification rate increased by 10.0 % and 7.1 % under NFM_{280} compared with PFM_{280} and BFM_{280} in both years, and the order was NF_{280}, BF_{280}, and PF_{280} (Table 3). CNU among all film treatments was lowest under NFM_{280} due to low root water uptake caused by high soil evaporation, despite high NO_3-N accumulated in the upper soil layer (0 − 40 cm). Average CNU in 2016 and 2017 under BFM_{280}, PFM_{280}, and NFM_{280} were 175, 192, and 136 kg ha^{-1}, respectively. Additionally, the higher the mulching area, the higher the NO_3-N

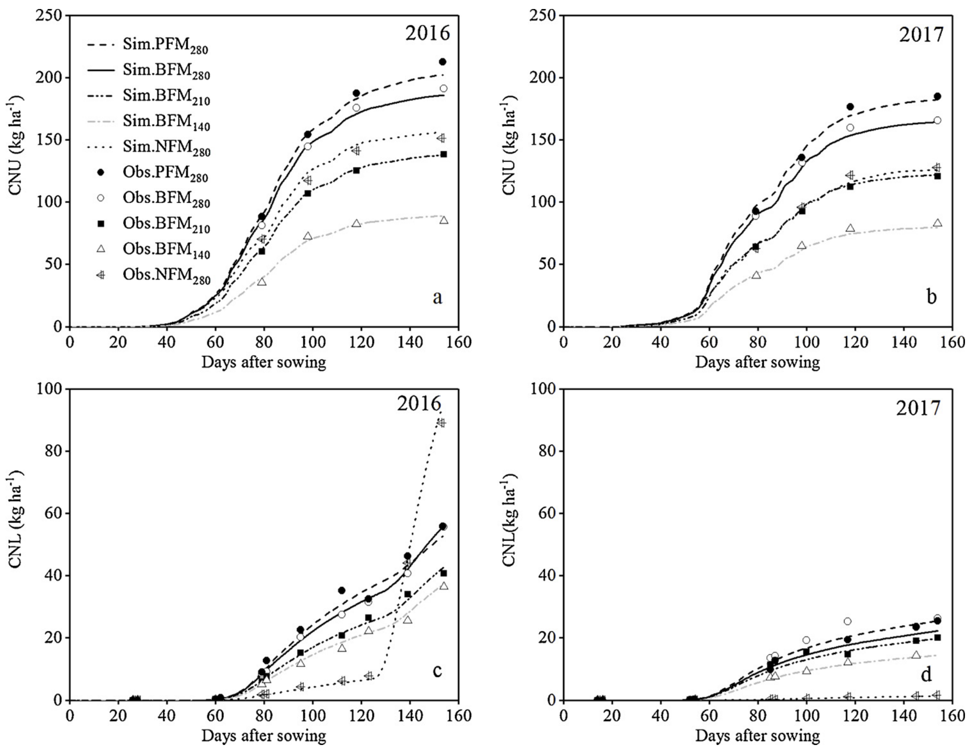

Fig. 5. Cumulative simulated and observed NO_3-N uptake (CNU, top) in 2016 (a) and 2017 (b) and cumulative NO_3-N leaching (CNL, bottom) at depths of 100 cm in 2016 (c) and 2017 (d) under plastic film mulching (PFM_{280}), biodegradable film mulching (BFM_{280}), and no film mulching (NFM_{280}) with an application of 280 kg ha^{-1} of the N-fertilizer, and biodegradable film mulching with applications of 210 kg ha^{-1} (BFM_{210}) and 140 kg ha^{-1} (BFM_{140}) of the N-fertilizer.

leaching, which was 22.3, 25.5, and 1.4 kg ha^{-1} under BFM_{280}, PFM_{280}, and NFM_{280}, respectively, in 2017 (Table 3).

A different pattern occurred in 2016 due to intensive rainfall during the late growing stage, with NO_3-N leaching 6.5 % and 77.8 % higher under BFM_{280} and NFM_{280}, respectively than under PFM_{280}. The opposite results were obtained for residual soil NO_3-N compared to CNL. Residual N under BFM_{280} and NFM_{280} increased by 14.3 and 8.1 kg ha^{-1}, respectively, compared to PFM_{280} in 2016, and by 15.5 and 91.5 kg ha^{-1}, respectively, in 2017. Moreover, the crop yield increased on average in two growing seasons by 50.8 % and 67.9 % under BFM_{280} and PFM_{280} compared with NFM_{280}. The average NUE in two growing seasons under BFM_{280} and PFM_{280} increased by 14.4 % and 15.6 % compared to NFM_{280}. Thus, while there were no significant differences in corn yields, NO_3-N leaching, and NUE under the BFM_{280} and PFM_{280} scenarios, all these values were much better than under NFM_{280}.

N uptake, NO_3-N leaching, and residual NO_3-N decreased with a decrease in the N-fertilizer application (Table 3). Average CNU in 2016 and 2017 under BFM_{210} and BFM_{140} compared with BFM_{280} decreased by 25.8 % and 51.8 %, respectively, CNL decreased by 23.1 % and 36.2 %, and residual NO_3-N declined by 25.2 % and 56.2 %, respectively. The highest NUE (the average value of 50.9 kg kg^{-1} for two years) was found under BFM_{210}, which represented an increase of 1.2 % and 12.5 % compared with BFM_{280} and BFM_{140}, respectively. The crop yield should increase when the N-fertilizer amount is enhanced in a suitable range: an average increase in corn yield was 73.2 % when the N-fertilizer application was increased from 140 to 210 kg ha^{-1}, and 33.3 % when from 210 to 280 kg ha^{-1}.

4. Discussion

4.1. Efficiency of HYDRUS (2D/3D)

Since the establishment of a reasonable irrigation or fertilization strategy requires precise knowledge of soil water and N dynamics, many field experiments would have to be conducted to obtain such information, which would be highly time-consuming and costly. Therefore, HYDRUS (2D/3D) has been widely used in the literature to simulate different irrigation and fertilization strategies to find such

Table 3
Simulated components of the N balance, observed corn yields, and the N use efficiency (NUE) under plastic film mulching (PFM_{280}), biodegradable film mulching (BFM_{280}), and no film mulching (NFM_{280}) with an application of 280 kg ha^{-1} of the N-fertilizer, and biodegradable film mulching with applications of 210 kg ha^{-1} (BFM_{210}) and 140 kg ha^{-1} (BFM_{140}) of the N-fertilizer. NUE: yield (kg ha^{-1}) divided by N uptake by crop (kg ha^{-1}). Different letters in the same column indicate a significant difference ($P < 0.05$) among treatments.

Year		N balance components (kg ha^{-1})						Yield (kg ha^{-1})	NUE (kg kg^{-1})
		Nitrification	Initial	Applied	Crop uptake	Leaching	Residual		
2016	PFM_{280}	37.6	44.8	179.2	202.1	52.7	6.8	10759.6 a	53.2
	BFM_{280}	38.9	44.8	179.2	185.7	56.1	21.1	9821.5 a	52.9
	BFM_{210}	29.2	33.6	134.4	137.7	42.8	16.7	7376.4 b	53.6
	BFM_{140}	19.5	22.4	89.6	88.9	37.3	5.3	4228.2 c	47.6
	NFM_{280}	40.5	44.8	179.2	155.9	93.7	14.9	7584.3 b	48.6
2017	PFM_{280}	33.7	44.8	179.2	182.2	25.5	53.2	8814.7 b	48.4
	BFM_{280}	34.3	44.8	179.2	164.1	22.3	68.7	7826.5 b	47.7
	BFM_{210}	24.2	33.6	134.4	121.8	17.5	50.5	5867.1 bc	48.2
	BFM_{140}	16.1	22.4	89.6	79.6	12.7	34	3413.8 d	42.9
	NFM_{280}	37.9	44.8	179.2	115.8	1.4	144.7	4545.4 c	39.3

optimal schemes, and it has been shown that this model can well capture temporal and spatial water and/or N dynamics (Ramos et al., 2012; Saglam et al., 2017; Karandish and Šimůnek, 2017; Everton et al., 2019). For example, Zhang et al. (2015) used HYDRUS (2D/3D) to evaluate different drip irrigation and fertigation strategies carried out in field experiments, and they reported the RMSE (between the model and data) ranging from 11.5 to 20.25 mg kg^{-1} for nitrate concentrations. Karandish and Šimůnek (2017) used the model to simulate drip irrigation for 11 irrigation levels and 8 nitrogen fertilization rates and indicated that the simulated NO_3-N concentrations agreed well with observed values with the RMSE ranging from 1.07 to 7.73 mg L^{-1}, and MBE ranging from -3.81-5.13 mg L^{-1}. Additionally, the subsurface transport of nitrate under three different initial nitrate concentrations was evaluated using HYDRUS (2D/3D) by Xie et al. (2019). Their research demonstrated excellent model performance with NSE of 0.744 and RMSE of 35.6 mg L^{-1} during the validation period.

However, the above-mentioned studies mainly focused on NO_3-N concentrations simulated under drip irrigation with no film mulching or under surface irrigation. This study represents the first study that both calibrated and validated HYDRUS (2D/3D) for different N-fertilizer application levels under biodegradable film mulching, obtaining the accuracy for the validation period that meets standard requirements with the *RMSE*, R^2, and *NSE* of 0.01-0.08 mg cm^{-3}, 0.62-0.87, and 0.68-0.94, respectively. HYDRUS (2D/3D) can thus be used to successfully simulate the NO_3-N movement in a drip-irrigated field with biodegradable film mulching.

4.2. Soil NO_3-N movement and distribution in the film mulching field

During the late growing season, soil evaporation, SWCs, and NO_3-N concentrations in the topsoil under biodegradable film mulching (BFM) were significantly different from those under plastic film mulching (PFM). The difference between these values under BFM and PFM increased in response to an increase in the disintegration of the biodegradable film. It can be seen that the movement and distribution of NO_3-N in the soil profile is mainly influenced by the soil water movement that is greatly affected by soil evaporation (Hillel, 1981; Lei, 1988; Li et al., 2015a,b). For example, high soil evaporation decreases soil water contents (SWC) and increases NO_3-N concentrations in the upper soil layer (Karandish and Šimůnek, 2017). Additionally, the capillary water movement may also enhance and directly accumulate NO_3-N in the topsoil. Film mulching may cut off the heat exchange between the atmosphere and the soil surface, reduce surface net radiation, decrease soil evaporation, increase SWCs, and decrease NO_3-N concentrations in the topsoil compared with no film mulching (NFM) (Monday et al., 2015; Ospanbayev et al., 2017; He et al., 2018).

There were no apparent differences during the early crop growth stage in NO_3-N distributions between BFM and PFM. Similarly, while SWCs under BFM and PFM were similar during the early crop growth stage (Saglam et al., 2017; Gu et al., 2017), SWCs under BFM were markedly lower than under PFM during DAS 150–240 due to the disintegration of the biodegradable film (Gu et al., 2017). Wang et al. (2019a,b) also reported that soil evaporation and soil water losses were enhanced by BFM compared with PFM at the late growth stages (DAS 120–180). Additionally, NO_3-N concentrations in the 0 − 20 cm soil layer under BFM were 25.7 % lower than under PFM based on the analysis of soil physicochemical properties and measured enzyme activities (Huang et al., 2019). However, different results were obtained in our experiment compared to those of Huang et al. (2019) due to differences in annual precipitations (103 mm in our experimental region and 430 mm in Huang et al., 2019). It can be expected that higher rainfall would cause higher NO_3-N losses from the upper soil layer. In this study, i.e., in the experimental region with low precipitation, the NO_3-N concentrations in the topsoil layer under BFM_{280} was 6.8 % and 3.9 % higher than under PFM_{280} during DAS 79–155 in 2016 and DAS 93–154 in 2017, respectively, but they were much lower than under NFM_{280} (Fig. 3, Table 3). The maximum difference between BFM_{280} and PFM_{280} occurred on the last day of the experiment with the 55.1 % disintegration of the biodegradable film, and the average NO_3-N concentrations in both years under BFM_{280} and PFM_{280} was 0.077 and 0.075 mg cm^{-3}, respectively (Fig. 3).

Furthermore, the NO_3-N concentrations in the upper soil layer (0 − 40 cm soil layer) under BFM_{280} decreased by 12.5 % compared to that under PFM_{280} on DAS 118 (one day after rainfall) during the late growing season. The cause of this phenomenon was that the movement of soil water and NO_3-N was significantly influenced by intensive rainfall that carried NO_3-N toward the deep soil layer. Similar findings were reported by Haraguchi et al. (2004), who found that large NO_3-N discharge occurred in the ridge-mulch treatment during three days after heavy rainfall, in which cumulative precipitation exceeded 10 mm. They also reported that daily NO_3-N leaching in the ridge-mulch treatment was twice as large as in the full-mulch treatment.

4.3. Analysis of N balance components

4.3.1. N balance components in the soil profile under film mulching

An increase of air and oxygen contents in response to a decrease in SWCs (e.g., Šimůnek and Suarez, 1993; Suarez and Šimůnek, 1993) results in intensive nitrification (Lei, 1988). Average nitrification in 2016 and 2017 under PFM_{280} was 2.9 % lower than under BFM_{280} (Table 3) due to the disintegration of the biodegradable film during the late growing season. The reason is that the disintegration of the biodegradable film decreased SWCs in the topsoil and increased nitrification. Similarly, Fernando et al. (2002) showed that nitrification under BFM was 12 % higher than under PFM.

N uptake is, in general, both an active and passive process (Marschner, 2013). However, since the passive component is often a dominant process, only this component of N uptake is often considered in the HYDRUS modeling (Filipovic et al., 2016; Karandish and Šimůnek, 2017; Saglam et al., 2017). There are significant differences in root water uptake for the BFM, PFM, and NFM scenarios, which also determines root solute uptake. Since passive N uptake is mainly influenced by root water uptake and soil NO_3-N concentrations, N uptake increases with an increase in NO_3-N concentrations under the same irrigation scenario. Therefore, CNU for an incomplete film mulch treatment was lower than for a complete film mulching treatment, with CNU under NFM lowest from all film treatments (Fig. 5, Table 3).

In our study, the crop yield under BFM_{280} was slightly lower compared to that under PFM_{280} because of the lower CNU (Table 3). The crop yield in general increases with an increase in transpiration and N uptake, independently of the presence or absence of film mulching (Ramos et al., 2012; Filipovic et al., 2016). Wang et al. (2019a,b) reported similar results, showing that PFM performed best in enhancing the cotton yield, while BFM increased cotton yield by 21.3 % and 12.1 % compared with NFM in wetter and drier years, respectively. However, there were also opposite conclusions that the crop yield under NFM is higher than under PFM (Filipovic et al., 2016), likely due to higher SWCs under NFM in the experimental area with a humid climate.

When the mulching area increased, NO_3-N leaching from the soil profile also increased. For example, CNL in 2016 for PFM_{280}, BFM_{280}, and NFM_{280} was 52.7, 56.1, and 93.7 kg ha^{-1}, respectively. Romic et al. (2003) similarly indicated that NO_3-N leaching at the end of the harvest under PFM, BFM, and NFM was 10, 18, and 26 kg ha^{-1}, respectively.

4.3.2. N balance components in the soil profile for different N-fertilizer application levels

Nitrate is a significant N source taken up from the soil by crops. Some studies have shown that applying reasonable amounts of the N-fertilizer was essential to protect agricultural ecological environments (Filipovic et al., 2016; Karandish and Šimůnek, 2017; Azad et al., 2018). In general, higher N-fertilizer applications can increase crop N uptake and yield (Li et al., 2004; Gheysari et al., 2009; Chen et al., 2018). For example, in this study, N uptake under BFM_{280} (a higher N-fertilizer application) increased by 25.8 and 51.8 % compared with BFM_{210} (a medium N-fertilizer application) and BFM_{140} (a low N-fertilizer application), respectively. However, higher N-fertilizer applications can easily cause more NO_3-N leaching and higher residual N concentrations, which may lead to serious pollution of groundwater environments, especially in regions with a shallow groundwater table (Marianne et al., 2013). Moreover, residual N concentrations generally increased with an increase in the N-fertilizer application. For example, Kim et al. (2014) reported an increase in the NO_3-N concentration of 0.0002 mg cm^{-3} with a unit increase in the N-fertilizer application under plastic film mulching. In our study, the NO_3-N concentrations increased by 0.0003 mg cm^{-3} under biodegradable film mulching, because evaporation under biodegradable film mulching was higher than under plastic film mulching. When the NO_3-N concentration in the soil profile is higher than a certain threshold, crop growth can be restricted, and the N use efficiency (NUE) can decrease (Hossain et al., 2018; Chen et al., 2018; Wang et al., 2019a,b). In this study, the NUE under BFM_{280} decreased by 1.2 % compared to BFM_{210}. Similar results were found by Yu and Ehrenfeld (2009), who noted that excessive N applications accelerated soil moisture depletion due to excessive vegetative growth and higher evapotranspiration demand, making the crop prone to the drought stress. On the other hand, lower applications of the N-fertilizer can produce a decrease in NO_3-N leaching and residual NO_3-N, but may not meet crop growth requirements, and cause low economic efficiency (Kumar et al., 2019).

Therefore, only a reasonable N-fertilizer amount can improve the NUE. In this study, the highest NUE of 50.9 kg kg^{-1} (an average for two years) was found under BFM_{210}, which represented an increase of 1.2 % and 12.5 % compared with BFM_{280} and BFM_{140}, respectively. An application of 210 kg ha^{-1} of the N-fertilizer was the best strategy for corn in a sandy region, which was similar to the research of Karandish and Šimůnek (2017) in the semi-arid region.

5. Conclusions

The N dynamic under BFM_{280}, PFM_{280}, and NFM_{280} was evaluated both experimentally and using numerical modeling with HYDRUS (2D/3D). The model was successfully calibrated and validated using observed NO_3-N concentrations from 2016 and 2017, respectively, obtaining the accuracy for the validation period that meets standard requirements with the *RMSE*, R^2, and *NSE* of 0.01-0.08 mg cm^{-3}, 0.62-0.87, and 0.68-0.94, respectively. There were only negligible differences in NO_3-N concentrations in the soil profile, CNU, and CNL at a depth of 100 cm between BFM_{280} and PFM_{280} during the early growing season (DAS 0–78 in 2016, DAS 0–92 in 2017), but there were quite substantial differences compared with NFM_{280}. The NO_3-N concentrations in the upper soil layer (0 − 40 cm) under BFM_{280} were higher than under PFM_{280} due to the disintegration of the biodegradable film. N uptake and NO_3-N leaching decreased with a decrease in the mulching area from PFM_{280} to BFM_{280}, and NFM_{280}. Additionally, NO_3-N leaching was greatly affected by intensive rainfall when no or little film mulching was present at the soil surface. Film mulching thus produced a significant advantage compared to no film mulching, While NO_3-N concentrations, N uptake, and NO_3-N leaching all increased under BFM with an increase in the N-fertilizer application, the highest NUE was found for BFM_{210}. Therefore, a biodegradable film can represent a good alternative to a plastic film in arid regions to avoid plastic pollution. The application of 210 kg ha^{-1} of the N-fertilizer with BFM was an optimal scenario in a sandy farmland.

Declaration of Competing Interest

The authors declare that they have no known competing financial interests or personal relationships that could have appeared to influence the work reported in this paper.

Acknowledgments

This research was jointly supported by the National Natural Science Foundation of China (51539005, 51669020, and 51469022), and the Natural Sciences Foundation of Inner Mongolia (2016JQ06).

References

Allen, R., Pereira, L.S., Raes, D., Smith, M., 1998. Crop Evapotranspiration: Guidelines for Computing Crop Requirements. FAO Irrigation and Drainage Paper No. 56. FAO, Rome.

Berger, S., Kim, Y., Kettering, J., Gebauer, G., 2013. Plastic mulching in agriculture—-friend or foe of N_2O emissions? Agric. Agric., Ecosyst. Environ., Appl. Soil Ecol. 167, 43–51. https://doi.org/10.1016/j.agee.2013.01.010.

Bremner, J., Keeney, D., 1965. Steam distillation methods for determination of ammonium, nitrate and nitrite. Anal. Chim. Acta 32, 485–495. https://doi.org/10.1016/S0003-2670(00)88973-4.

Campbell, G., Norman, J., 1989. The Description and Measurement of Plant Canopy Structure. Plant Canopies: Their Growth Form, and Function. Society for Experimental Biology. Cambridge University Press, Cambridge, pp. 1–19. https://doi.org/10.1017/cbo9780511752308.002.

Castaldelli, G., Nicolò, C., Tamburini, E., Vincenzi, F., Micòl, M., 2018. Soil type and microclimatic conditions as drivers of urea transformation kinetics in maize plots. Catena 166, 200–208. https://doi.org/10.1016/j.catena.2018.04.009.

Chen, J., Wang, P., Ma, Z., Liu, X., Liu, T., Kadambot, H., Siddique, 2018. Optimum water and nitrogen supply regulates root distribution and produces high grain yields in spring wheat (*Triticum aestivum L.*) under permanent raised bed tillage in arid northwest China. Soil Tillage Res. 181, 117–126. https://doi.org/10.1016/j.still.2018.04.012.

Chen, N., Li, X.Y., Šimůnek, J., Shi, H.B., Ding, Z.J., Peng, Z.Y., 2019. Evaluating the effects of biodegradable film mulching on soil water dynamics in a drip-irrigated field. Agric. Water Manage. 226, 105788. https://doi.org/10.1016/j.agwat.2019.105788.

Cote, C., Bristow, K., Charlesworth, P., Cook, F., Charlesworth, P., 2003. Analysis of soil wetting and solute transport in subsurface trickle irrigation. Irrig. Sci. 22, 143–156. https://doi.org/10.1007/s00271-003-0080-8.

Suarez, D.L., Šimůnek, J., 1993. Modeling of carbon dioxide transport and production in soil: 2. Parameter selection, sensitivity analysis, and comparison of model predictions to field data. Water Resour. Res. 29 (2), 499–513. https://doi.org/10.1029/92wr02226.

Daryanto, S., Wang, L., Jacinthe, P., 2017. Can ridge-furrow plastic mulching replace irrigation in dryland wheat and maize cropping systems? Agric. Water Manage. 190, 1–5. https://doi.org/10.1016/j.agwat.2017.05.005.

Dlamini, P., Ukoh, I., Van Rensburg, L., Du Preez, C., 2017. Reduction of evaporation from bare soil using plastic and gravel mulches and assessment of gravel mulch for partitioning evapotranspiration under irrigated canola. Arid. Soil Res. Rehabil. 55 (3), 222. https://doi.org/10.1071/sr16098.

Dong, H., Liu, T., Li, Y., Liu, H., Wang, D., 2013. Effects of plastic film residue on cotton yield and soil physical and chemical properties in Xinjiang. Trans. Chin. Soc. Agric. Eng. 29 (8), 91–99.

Fawibe, O., Honda, K., Taguchi, Y., 2019. Greenhouse gas emissions from rice field cultivation with drip irrigation and plastic film mulch. Nutr. Cycling Agroecosyst. 113, 51–62. https://doi.org/10.1007/s10705-018-9961-3.

Feddes, R., Kowalik, P., Zaradny, H., 1978. Simulation of Field Water Use and Crop Yield. John Wiley & Sons, New York. https://doi.org/10.1002/jpln.19801430219.

Fernando, W., Suyama, K., Itoh, K., Tanaka, H., Yamamoto, H., 2002. Degradation of an acylated starch-plastic mulch film in soil and impact on soil microflora. Soil Sci. Plant Nutr. 48 (5), 701–709. https://doi.org/10.1080/00380768.2002.10409260.

Filipovic, V., Romic, D., Romic, M., Borosic, J., Filipovic, L., Mallmann, F., Robinson, D., 2016. Plastic mulch and nitrogen fertigation in growing vegetables modify soil temperature, water and nitrate dynamics: experimental results and a modeling study. Agric. Water Manage. 176, 100–110. https://doi.org/10.1016/j.agwat.2016.04.020.

Gao, H., Yan, C., Liu, Q., Ding, W., Chen, B., Li, Z., 2019. Effects of plastic mulching and plastic residue on agricultural production: a meta-analysis. Sci. Total Environ. 651, 484–492. https://doi.org/10.1016/j.scitotenv.2018.09.105.

Gheysari, M., Mirlatifi, S.M., Homaee, M., Asadi, M.E., Hoogenboom, G., 2009. Nitrate leaching in a silage maize field under different irrigation and nitrogen fertilizer rates. Agric. Water Manage. 96, 946–954. https://doi.org/10.1016/j.agwat.2009.01.005.

Gu, X., Li, Y., Du, Y., 2017. Biodegradable film mulching improves soil temperature, water and seed yield of winter oilseed rape (*Brassica napus* L.). Soil Tillage Res. 171, 42–50. https://doi.org/10.1016/j.still.2017.04.008.

Guo, H., Li, S.E., Kang, S.Z., Du, T.S., Tong, L., Ding, R.S., 2019. Annual ecosystem respiration of maize was primarily driven by crop growth and soil water conditions. Agric. Ecosyst. Environ. 272, 254–265. https://doi.org/10.1016/j.agee.2018.11.026.

Haraguchi, T., Marui, A., Yuge, K., Nakano, Y., Mori, K., 2004. Effect of plastic-film mulching on leaching of nitrate nitrogen in an upland field converted from paddy. Paddy Water Environ. 2 (2), 67–72. https://doi.org/10.1007/s10333-004-0042-7.

Hanson, B., Šimůnek, J., Hopmans, J., 2006. Evaluation of urea–ammonium–nitrate fertigation with drip irrigation using numerical modeling. Agric. Water Manage. 86, 102–113. https://doi.org/10.1016/j.agwat.2006.06.013.

He, Q., Li, S., Kang, S., Yang, H., Qin, S., 2018. Simulation of water balance in a maize

field under film-mulching drip irrigation. Agric. Water Manage. 210, 252–260. https://doi.org/10.1016/j.agwat.2018.08.005.
Henry, Y.S., Sreejata, B., Marie, E.E., Andy, I.B., Jennifer, M.D., Sean, M.S., Carol, A.M., John, P.R., Markus, F., 2019. Impacts of biodegradable plastic mulches on soil health. Agric. Ecosyst. Environ. 273, 36–49. https://doi.org/10.1016/j.agee.2018.12.002.
Hillel, D., 1981. Soil and Water, Physical Principles and Processes. Agricultural Press, Beijing. https://doi.org/10.1016/b978-0-124-77915-0.x5001-5.
Hossain, S., Lixue, W., Liu, H., 2018. Improved greenhouse cucumber production under deficit water and fertilization in northern china. Int. J. Agric. Biol. Eng. 11 (4), 58–64. https://doi.org/10.25165/j.ijabe.20181103.3566.
Huang, F., Liu, Z., Mou, H., Li, J., Zhang, P., 2019. Impact of farmland mulching practices on the soil bacterial community structure in the semiarid area of the loess plateau in China. Eur. J. Soil Biol. 8–15. https://doi.org/10.1016/j.ejsobi.2019.04.001.
Ibarra-Jiménez, Luis, Hugolira-Saldivar, R., Valdez-Aguilar, Luis Alonso, Río, J.L.D., 2011. Colored plastic mulches affect soil temperature and tuber production of potato. Acta Agric. Scand. 61, 365–371. https://doi.org/10.1016/j.ejsobi.2019.04.001.
Jiang, X., Liu, W., Wang, E., Zhou, T., Xin, P., 2017. Residual plastic mulch fragments effects on soil physical properties and water flow behavior in the Minqin Oasis. northwestern China. Soil Tillage Res 166, 100–107. https://doi.org/10.1016/j.still.2016.10.011.
Jordi, G., Oriol, M., Candela, L., Serrano, L., 1995. Nitrate leaching and strawberry production under drip irrigation management. Agric. Ecosyst. Environ. 56 (2), 121–135. https://doi.org/10.1016/0167-8809(95)00620-6.
Karandish, F., Šimůnek, J., 2017. Two-dimensional modeling of nitrogen and water dynamics for various N-managed water-saving irrigation strategies using HYDRUS. Agric. Water Manage 193, 174–190. https://doi.org/10.1016/j.agwat.2017.07.023.
Khalil, H., Chong, E., Owolabi, F., 2018. Microbial-induced $CaCO_3$ filled seaweed-based film for green plasticulture application. J. Cleaner Prod 199, 150–163. https://doi.org/10.1016/j.jclepro.2018.07.111.
Kim, Y., Berger, S., Kettering, J., Tenhunen, J., Haas, E., Kiese, R., 2014. Simulation of N_2O emissions and nitrate leaching from plastic mulch radish cultivation with LandscapeDNDC. J. Gynecol. Res. Obstet. 29 (3), 441–454. https://doi.org/10.1007/s11284-014-1136-3.
Kumar, V., Sharma, J., Kumar, M., Singh, S., Kumar, A., 2019. Mulches and nutrients affect the soil environment, crop performance and profitability of cauliflower. J. Anima. P. Sci. 29 (1), 194–204.
Lazarovitch, N., Pollton, M., Furman, A., Warrick, A., 2009. Water distribution under trickle irrigation predicted using artificial neural networks. J. Eng. Math. 64, 207–218. https://doi.org/10.1007/s10665-009-9282-2.
Lei, Z., 1988. Soil Water Dynamics. Tsinghua University Press, Beijing.
Li, J., Zhang, J., Rao, M., 2004. Wetting patterns and nitrogen distributions as affected by fertigation strategies from a surface point source. Agric. Water Manage. 67, 89–104. https://doi.org/10.1016/s0378-3774(04)00043-5.
Li, X., Shi, H., Šimůnek, J., Gong, X., Peng, Z., 2015a. Modeling soil water dynamics in a drip-irrigated intercropping field under plastic mulch. Irrig. Sci. 33 (4), 289–302. https://doi.org/10.1007/s00271-015-0466-4.
Li, X., Šimůnek, J., Shi, H., Yan, J., Peng, Z., Gong, X., 2017. Spatial distribution of soil water, soil temperature, and plant roots in a drip-irrigated intercropping field with plastic mulch. Eur. J. Agron. 83, 47–56. https://doi.org/10.1016/j.eja.2016.10.015.
Li, Y., Šimůnek, J., Jing, L., Zhang, Z., Ni, L., 2014. Evaluation of water movement and water losses in a direct-seeded-rice field experiment using Hydrus-1D. Agric. Water Manage. 142, 38–46. https://doi.org/10.1016/j.agwat.2014.04.021.
Li, Y., Šimůnek, J., Zhang, Z., Jing, L., Ni, L., 2015b. Evaluation of nitrogen balance in a direct-seeded-rice field experiment using Hydrus-1D. Agric. Water Manage. 148, 213–222. https://doi.org/10.1016/j.agwat.2014.10.010.
Liu, E., He, W., Yan, C., 2014. 'White revolution' to 'white pollution'—agricultural plastic film mulch in China. Environ. Res. Lett. 9, 091001. https://doi.org/10.1088/1748-9326/9/9/091001.
Ma, D., Chen, L., Qu, H., Wang, Y., Misselbrook, T., Jiang, R., 2018. Impacts of plastic film mulching on crop yields, soil water, nitrate, and organic carbon in northwestern China: a meta-analysis. Agric. Water Manage. 202, 166–173. https://doi.org/10.1016/j.agwat.2018.02.001.
Mari, A., Pardo, G., Cirujeda, A., 2019. Economic Evaluation of biodegradable plastic films and paper mulches used in open-air grown pepper (*Capsicum annum L.*) crop. Agronomy Basel (Basel) 9 (1), 36. https://doi.org/10.3390/agronomy9010036.
Marianne, R., Svenja, B., Janine, K., Bernd, H., Sven, F., 2013. The effect of fertilizer best management practices on nitrate leaching in a plastic mulched ridge cultivation system. Agric. Ecosyst. Environ. 169, 21–32. https://doi.org/10.1016/j.agee.2013.02.006.
Marschner, P., 2013. Marschner's Mineral Nutrition of Higher Plants (Second Edition). Science Press.
Monday, T., Foshee, W., Blythe, E., Wehtje, G., Gilliam, C., 2015. Yellow nutsedge (*cyperus esculentus*) control and tomato response to application methods of drip-applied herbicides in polyethylene-mulched tomato. Weed Technol. 29 (3), 625–632. https://doi.org/10.1614/wt-d-15-00025.1.
Monteiro, R., Coelho, R., Whopmans, J., Lennartz, B., 2013. Water consumption and soil water distribution in melon crop with mulching and in a protected environment. Rev. Bras. Frutic. 35 (2), 555–564. https://doi.org/10.1590/s0100-29452013000200026.
Monteith, J.L., 1981. Evaporation and surface temperature. Q. J. R. Meteorol. Soc. 107, 1–27. https://doi.org/10.1002/qj.49710745102.
Moreno, M., Mora, S., Villena, J., Campos, J., Moreno, C., 2017. Deterioration pattern of six biodegradable, potentially low-environmental impact mulches in field conditions. J. Environ. Manage. 200, 490–501. https://doi.org/10.1016/j.jenvman.2017.06.007.
Mueller, S.M., Vyn, T.J., 2018. Physiological constraints to realizing maize grain yield recovery with silking-stage nitrogen fertilizer applications. Field Crops Res. 228, 102–109. https://doi.org/10.1016/j.fcr.2018.08.025.
Nakamura, K., Harter, T., Hirono, Y., Horino, H., Mitsuno, T., 2004. Assessment of root zone nitrogen leaching as affected by irrigation and nutrient management practices. Vadose Zone J. 3, 1353–1366. https://doi.org/10.2113/3.4.1353.
Nasrullah, H.M., Khan, M.B., Ahmad, R., Ahmad, S., Hanif, M., Nazeer, W., 2011. Sustainable cotton production and water economy through different planting methods and mulching techniques. Pak. J. Bot. 43 (4), 1971–1983.
Novello, V., Palma, L., 2008. Growing grapes under cover. Acta Hortic. 785, 353–362. https://doi.org/10.17660/actahortic.2008.785.44.
Vázquez, N., Pardo, A., Suso, M.L., Quemada, M., 2006. Drainage and nitrate leaching under processing tomato growth with drip irrigation and plastic mulching. Agric. Ecosyst. Environ. 112 (4), 313–323. https://doi.org/10.1016/j.agee.2005.07.009.
Ospanbayev, Z., Kurmanbayeva, M., Abdukadirova, Z., Doszhanova, A., Nazarbekova, S., Inelova, Z., Ablaikhanova, N., Kenenbayev, S., Musina, A., 2017. Water use efficiency of rice and soybean under drip irrigation with mulch in the south-east of Kazakhstan. Applied Eco. Envir. Res. 15, 1581–1603. https://doi.org/10.15666/aeer/1504_15811603.
Qi, Y., Yang, X., Mejia, P., Huerta, L., Beriot, N., Gertsen, H., Garbeva, P., Geissen, V., 2018. Macro- and micro-plastics in soil-plant system: effects of plastic mulch film residues on wheat (*Triticum aestivum*) growth. Sci. Total Environ. 645, 1048–1056. https://doi.org/10.1016/j.scitotenv.2018.07.229.
Qin, S., Li, S., Kang, S., 2019. Transpiration of female and male parents of seed maize in northwest China. Agric. Water Manage. 213, 397–409. https://doi.org/10.1016/j.agwat.2018.10.016.
Ramos, T., Šimůnek, J., Gonalves, M., Martins, J., Prazeres, A., Pereira, L., 2012. Two-dimensional modeling of water and nitrogen fate from sweet sorghum irrigated with fresh and blended saline waters. Agric. Water Manage 111, 87–104. https://doi.org/10.1016/j.agwat.2012.05.007.
Ravikumar, V., Vijayakumar, G., Šimůnek, J., Chellamuthu, S., Santhi, R., Appavu, K., 2011. Evaluation of fertigation scheduling for sugarcane using a vadose zone flow and transport model. Agric. Water Manage. 98, 1431–1440. https://doi.org/10.1016/j.agwat.2011.04.012.
Romic, D., Romic, M., Borosic, J., Poljak, M., 2003. Mulching decreases nitrate leaching in bell pepper (*Capsicum annuum L.*) cultivation. Agric. Water Manage. 60, 87–97. https://doi.org/10.1016/s0378-3774(02)00168-3.
Ruidisch, M., Bartsch, S., Kettering, J., Huwe, B., Frei, S., 2013. The effect of fertilizer best management practices on nitrate leaching in a plastic mulched ridge cultivation system. Agric. Ecosyst. Environ. 169, 21–32. https://doi.org/10.1016/j.agee.2013.02.006.
Saglam, M., Sintim, H., Bary, A., Miles, C., Ghimire, S., Inglis, D., Flury, M., 2017. Modeling the effect of biodegradable paper and plastic mulch on soil water dynamics. Agric. Water Manage. 193, 240–250. https://doi.org/10.1016/j.agwat.2017.08.011.
Schaap, M., Leij, F., van Genuchten, M.Th., 2001. ROSETTA: a computer program for estimating soil hydraulic parameters with hierarchical pedotransfer functions. J. Hydrol. 251, 163–176. https://doi.org/10.1016/s0022-1694(01)00466-8.
Sharma, S., Leskovar, D., Crosby, K., Volder, A., 2017. Root growth dynamics and fruit yield of melon (*cucumis melo l*) genotypes at two locations with sandy loam and clay soils. Soil Tillage Res. 168, 50–62. https://doi.org/10.1016/j.still.2016.12.006.
Šimůnek, J., Suarez, D.L., 1993. Modeling of carbon dioxide transport and production in soil: 1. Model development. Water Resour. Res. 29 (2), 487–497. https://doi.org/10.1029/92wr02225.
Šimůnek, J., van Genuchten, M.T., Šejna, M., 2016. Recent developments and applications of the HYDRUS computer software packages. Vadose Zone J. 15, 25. https://doi.org/10.2136/vzj2016.04.0033.
Skaggs, T., Trout, T.J., Šimůnek, J., Shouse, P.J., 2004. Comparison of Hydrus-2D simulations of drip irrigation with experimental observations. J. Irrig. Drain. Eng. 130 (4), 304–310. https://doi.org/10.1061/(asce)0733-9437(2004)130:4(304).
Sun, T., Li, G., Ning, T., Zhang, Z., Mi, Q., Lai, R., 2018. Suitability of mulching with biodegradable film to moderate soil temperature and water and to increase photosynthesis and yield in peanut. Agric. Water Manage. 208, 214–223. https://doi.org/10.1016/j.agwat.2018.06.027.
Tafteh, A., Sepaskhah, A., 2012. Application of HYDRUS-1D model for simulating water and nitrate leaching from continuous and alternate furrow irrigated rapeseed and maize fields. Agric. Water Manage. 113, 19–29. https://doi.org/10.1016/j.agwat.2012.06.011.
Touchaleaume, F., Martin, C., Angellier, C., Chevillard, A., Cesar, G., Gontard, N., Gastaldi, E., 2016. Performance and environmental impact of biodegradable polymers as agricultural mulching films. Chemosphere 144, 433–439. https://doi.org/10.1016/j.chemosphere.2015.09.006.
Wang, H., Ju, X., Wei, Y., Li, B., Zhao, L., Hu, K., 2010. Simulation of bromide and nitrate leaching under heavy rainfall and high-intensity irrigation rates in North China Plain. Agric. Water Manage. 97, 1646–1654. https://doi.org/10.1016/j.agwat.2010.05.022.
Wang, H., Li, J., Cheng, M., Zhang, F., Wang, X., Fan, J., Wu, L., Fang, D., Zou, H., Xiang, Y., 2019a. Optimal drip fertigation management improves yield, quality, water and nitrogen use efficiency of greenhouse cucumber. Sci. Hortic. 243, 357–366. https://doi.org/10.1016/j.scienta.2018.08.050.
Wang, X., Xing, Y., 2016. Effects of mulching and nitrogen on soil nitrate-n distribution, leaching and nitrogen use efficiency of maize (*zea mays l*). PLoS One 11 (8), e0161612. https://doi.org/10.1371/journal.pone.0161612.
Wang, Z., Wu, Q., Fan, B., 2019b. Effects of mulching biodegradable films under drip irrigation on soil hydrothermal conditions and cotton (*Gossypium hirsutum L.*) yield. Agric. Water Manage. 213, 477–485. https://doi.org/10.1016/j.agwat.2018.10.036.
Wen, Y., 2005. The Functional Plastic Film. China Machine Press, Beijing, pp. 262.
Xie, M.X., Šimůnek, J., Zhang, Z.Y., Zhang, P.C., Xu, J.X., Lin, Q.M., 2019. Nitrate subsurface transport and losses in response to its initial distributions in sloped soils: an experimental and modelling study. Hydrol. Process. https://doi.org/10.1002/hyp.

13556. 15 p.
Yan, C., Liu, E., Shu, F., Liu, Q., Liu, S., He, W., 2014. Review of agricultural plastic mulching and its residual pollution and prevention measures in China. J. Agric. Res. Environ. 31, 95–102.
Yin, M., Li, Y., Fang, H., Chen, P., 2019. Biodegradable mulching film with an optimum degradation rate improves soil environment and enhances maize growth. Agric. Water Manage. 216, 127–137. https://doi.org/10.1016/j.agwat.2019.02.004.
Yu, S., Ehrenfeld, J.G., 2009. The effects of changes in soil moisture on nitrogen cycling in acid wetland types of the New Jersey Pinelands (USA). Soil Biol. Biochem. 41, 2394–2405. https://doi.org/10.1016/j.soilbio.2009.06.012.
Zhang, H., Liu, Q., Yu, X., Guoan, L., Wu, Y., 2012. Effects of plastic mulch duration on nitrogen mineralization and leaching in peanut (*arachis hypogaea*) cultivated land in the yimeng mountainous area, china. Agric. Ecosyst. Environ. 158, 164–171. https://doi.org/10.1016/j.agee.2012.06.009.
Zhang, J.J., Li, J.S., Zhao, B.Q., Li, Y.T., 2015. Simulation of water and nitrogen dynamics as affected by drip fertigation strategies. J. Integr. Agric. 14 (12), 2434–2445. https://doi.org/10.1016/s2095-3119(15)61231-x.
Zheng, M., Leib, B., Butler, D., Wright, W., Ayers, P., Hayes, D., Haghverdi, A., Grant, T., Vanchiasong, P., Muchoki, D., 2018. Assessing heat management practices in high tunnels to improve organic production of bell peppers. Sci. Hortic. 246, 928–941. https://doi.org/10.1016/j.scienta.2018.10.046.
Zhou, L., Feng, H., Zhao, Y., Qi, Z., Zhang, T., Si, B., 2017. Root-shoot regulation and yield of mulched drip irrigated maize on sandy soil. Int. J. Plant Prod. 11 (4), 461–475.